PROCEEDINGS OF SCIENCE

# Energy spectrum and composition measurements of cosmic rays from GRAPES-3 experiment

**F. Varsi**[*1,6†] **S. Ahmad**[1,4], **M. Chakraborty**[1,2], **A. Chandra**[1,4], **S.R. Dugad**[1,2], **S.K. Gupta**[1,2], **B. Hariharan**[1,2,3], **Y. Hayashi**[1,5], **S.S.R. Inbanathan**[1,3], **P. Jagadeesan**[1,2], **A. Jain**[1,2], **P. Jain**[1,6], **V.B. Jhansi**[1,2], **S. Kawakami**[1,5], **H. Kojima**[1,7], **S. Mahapatra**[1,8], **P.K. Mohanty**[1,2], **S.D. Morris**[1,2], **Y. Muraki**[1,9], **P.K. Nayak**[1,2], **A. Oshima**[1,7], **D. Pattanaik**[1,2], **P.S. Rakshe**[1,2], **K. Ramesh**[1,2], **B.S. Rao**[1,2], **L.V. Reddy**[1,2], **S. Sharma**[1,2], **S. Shibata**[1,2], **K. Tanaka**[1,10], **M. Zuberi**[1,2]

[1] *The GRAPES-3 Experiment, Cosmic Ray Laboratory, Raj Bhavan, Ooty 643001, India*
[2] *Tata Institute of Fundamental Research, Mumbai 400005, India*
[3] *The American College, Madurai 625002, India*
[4] *Aligarh Muslim Univeristy, Aligarh 202002, India*
[5] *Graduate School of Science, Osaka City University, Osaka 558-8585, Japan*
[6] *Indian Institute of Technology Kanpur, Kanpur 208016, India*
[7] *College of Engineering, Chubu University, Kasugai, Aichi 487-8501, Japan*
[8] *Utkal University, Bhuvaneshwar 751004, India*
[9] *Institute for Space-Earth Environmental Research, Nagoya University, Nagoya 464-8601, Japan*
[10] *Graduate School of Information Sciences, Hiroshima City University, Hiroshima 731-3194, Japan*

Precise measurements of the nuclear composition, and energy spectrum of primary cosmic rays at the 'knee' and beyond is essential to understand their astrophysical origin, acceleration, and properties of interstellar medium. The GRAPES-3 experiment located at Ooty in India is designed with a densely packed array of scintillator detectors. It measures cosmic rays from several TeV to over 10 PeV while providing a substantial overlap with direct experiments. The muon multiplicity distribution measured by the large area tracking muon detector associated with the array is sensitive to composition. Recently, we have attempted to measure the energy spectrum and composition from sub-TeV to over 10 PeV. The results obtained so far will be presented during the conference.

*36th International Cosmic Ray Conference -ICRC2019-*
*July 24th - August 1st, 2019*
*Madison, WI, U.S.A.*

[*] Speaker.
[†] fahim@iitk.ac.in





PoS(ICRC2019)449

## 1. The GRAPES-3 Eperiment

The GRAPES-3 (Gamma Ray Astronomy at PeV Energies Phase-3) experiment is located at Ooty (11.4° N, 76.7° E, 2200 m a.s.l.), India. The GRAPES-3 extensive air shower (EAS) array consists of 400 plastic scintillator detectors of 1 $m^2$ area each[1−2] and a large area tracking muon detector. A schematic of the array is shown in Figure 1. The scintillator array covers an area of 25000 $m^2$. The scintillator detectors are arranged in hexagonal geometry, to ensure the uniform selection of the EAS over the array, with an inter-detector seperation of 8 m. The 560 $m^2$ tracking muon detector consists of 3712 proportional counters (PRCs) each of length 600 cm and cross-section area of 10 cm × 10 cm. The PRCs are housed in 4 stations and each station has 4 modules. Each module has 4 orthogonal layers consisting of 58 PRCs in each layer[3]. It has an energy threshold of sec($\theta$) GeV for muons incident at zenith angle $\theta$. The fiducial area (14560 $m^2$) is shown by red dashed line. GRAPES-3 uses two level trigger. Level-0 trigger is a simple 3-line coincidence in 100 ns time window and level-1 trigger requires at least 10 detectors hit in 1 $\mu$s time window[1].

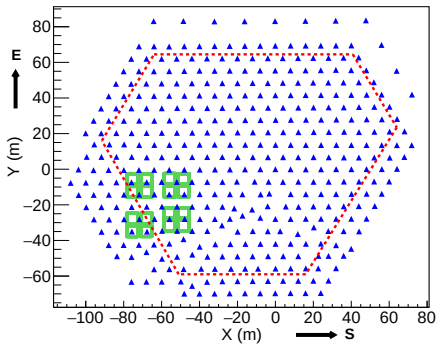


Figure 1: Schematic of GRAPES-3 EAS array. Plastic scintillator detectors (▲), tracking muon detector modules (□) and fiducial area (- - -) are shown.

Being a highly dense EAS array with an atmospheric overburden of ∼800 g cm$^{-2}$, the GRAPES-3 experiment is capable of observing any fine structure in the energy spectrum, if it exists, and could measure primary cosmic rays (PCRs) from several TeV to over 10 PeV, providing a substantial overlap with direct experiments. GRAPES-3 tracking muon detector is sensitive to PCRs composition measurements through muon multiplicity distribution.

## 2. Data selection

Data collected by GRAPES-3 array during 1 January - 31 December 2014 was used for the analysis. The total live time of data collection is ∼ 318.5 days. Total number of EAS recorded during live time is 9.7 ×10$^8$. The following event selection criteria are used to ensure the quality of the data. The number of showers remaining after applying all the cuts are 2.3 ×10$^8$.

1. Reconstruction output flag is used to define the quality of the reconstruction and only those EAS were selected for the analysis which satisfied reconstruction quality criteria.

2. The reconstructed cores must lie within the fiducial area. In this way, most of the improperly reconstructed EAS, due to EAS core landing near to the edge of the array can be avoided.

3. The reconstructed age parameter (s) was restricted between 0.5 and 1.7.

4. Zenith angle was restricted to ∼ 25° (1.0 ≤ sec$\theta$ < 1.1). The analysis was done in two different sec$\theta$ bins of bin-width 0.05. The results were then combined after sec$\theta$ correction by parameterization.

## 3. Simulations

A detailed simulation study was done to calculate the efficiency and acceptance for EAS detector array and energy calibration. Proton initiated EAS were produced by CORSIKA (version 7.69) simulation package using SIBYLL-2.3c and FLUKA hadronic interaction models for high and low energy, respectively. Data were generated in the energy range of 1 TeV to 10 PeV in 20 logarithmic energy bin of bin-width $10^{0.2}$ and zenith angle range of $0^\circ$ - $60^\circ$, following a power law with a spectral index of -2.5. The data were generated with energy cuts of 50 MeV, 10 MeV, 1 MeV and 1 MeV for hadrons, muons, electrons and photons, respectively. For the analysis, each shower was thrown in a circular area of radius 150 m from the center (-13.85 m, 6.29 m) of the GRAPES-3 EAS detector array with random core position. Each shower was reused 10 times to improve the statistics, which makes the total number of shower to be $1.2 \times 10^9$. The GEANT-4 package was used to simulate the detector response and a constant discriminator threshold of 0.5 particles was used for each detector.

### 3.1 Reconstruction of shower axis and shower parameters

The relative arrival time of particles and the energy deposited by the particles in each scintillator detector was recorded for every triggered shower. The relative arrival time of the EAS measured by different detectors were used to reconstruct the arrival direction of EAS by fitting them with a plane front. The shower parameters were obtained by fitting a lateral distribution function namely Nishimura-Kamata-Greisen (NKG) to the observed particle densities in the detectors. The NKG function is given by:

$$\rho(r,s,N_e) = \frac{N_e}{2\pi r_o^2} \frac{\Gamma(4.5-s)}{\Gamma(s)\Gamma(4.5-2s)} \left(\frac{r}{r_o}\right)^{(s-2)} \left(1+\frac{r}{r_o}\right)^{(s-4.5)} \qquad ...(1)$$

where $N_e$ is the shower size, s is the shower age, r is the lateral distance from shower core (X, Y). $r_0$ is the Moliere radius, for GRAPES-3, $r_0$ = 103 m.

### 3.2 Trigger efficiency, reconstruction efficiency and Acceptance

Further anlysis was carried out for 8 sec$\theta$ bins ranging from 1.00 to 1.40 with a bin-width of 0.05, and 20 logarithmic energy bins ranging from 1 TeV to 10 PeV of bin-width $10^{0.2}$. For each energy and sec$\theta$ bin, the trigger efficiency ($\varepsilon_T$) was calculated by the fraction of EAS having the shower core within the fiducial area that passes the level-0 and level-1 trigger conditions. The reconstruction efficiency ($\varepsilon_R$) was calculated by the fraction of triggered EAS that passes the reconstruction quality cut. Total efficiency ($\varepsilon$) was determined by the product of trigger and reconstuction efficiency. Due to limitations of the poissonian and binomial error caculation, the method presented in reference [4] is used to calculate the error in total efficiency. For a given sec$\theta$ bin, $n_i$ and $k_i$ are the number of EAS having the shower core within the fiducial area, and the number of EAS that pass both the trigger conditions and reconstruction quality cut, respectively, in the $i^{th}$ energy bin. Then the error in total efficiency ($\sigma_i$) in the $i^{th}$ energy bin is given as:

$$\sigma_i = \sqrt{\frac{(k_i+1)(k_i+2)}{(n_i+2)(n_i+3)} - \frac{(k_i+1)^2}{(n_i+2)^2}} \qquad ...(2)$$

Acceptance ($A_{acc}$) is represented as the product of the effective area and the effective viewing angle. Acceptance is also a function of direction and energy.

$$A_{acc}(E_T) = \frac{\pi A}{2} \sum_{k=1}^{n_\theta} \varepsilon_{tot}(E_T, \theta_k)(cos2\theta_k - cos2\theta_{k+1}) \qquad ...(3)$$

where A is the fiducial area, $n_\theta$ is the total number of angle bins and $\theta_k$ and $\theta_{k+1}$ are low and high edges of each angle bin, respectively. The trigger efficiency for all sec$\theta$ bins are shown in Figure 2(a) and the total acceptance ($1.0 \leq \sec\theta < 1.4$) for GRAPES-3 EAS array is shown in Figure 2(b). The trigger efficiency increases with energy of the PCRs because the PCRs of higher energy produce more number of secondary particles with relatively higher energy. Hence the probability of the trigger increases. For $1.0 \leq \sec\theta < 1.05$, the trigger efficiency increases from 0.06% at 1.2 TeV to 93% at 48.2 TeV. The trigger efficiency at a given energy decreases with increase in the zenith. It is due to the fact that with increase in zenith, the effective length travelled by the EAS increases and causes more attenuation of the EAS. Hence the probabilty of the trigger decreases. The acceptance for the GRAPES-3 EAS array is 4.8 $m^2$sr at 1.2 TeV and increases upto 21840 $m^2$sr at 760 TeV.

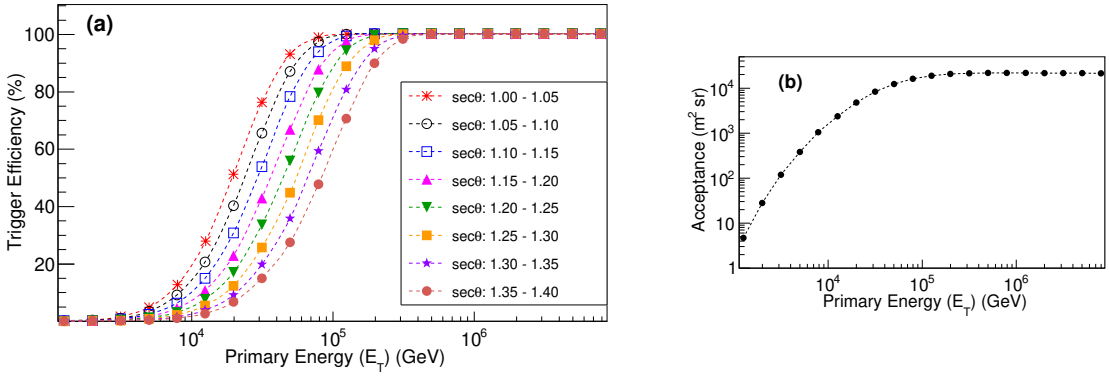


Figure 2: (a): Trigger efficiency for proton initiated EAS for different sec$\theta$ bins. (b): Total acceptance for GRAPES-3 EAS array.

### 3.3 Energy calibration

The shower size ($N_e$) is a measure of the energy of PCRs ($E_T$) particle. The conversion relation can be derived from simulation. The log-log profile plot of the $N_e$ and $E_T$ for $1.0 \leq \sec\theta < 1.05$ is shown in Figure 3(a). The variation is linear in the region having 100% trigger efficiency (region 1). In the region where the efficiency is less than 100% (region 2), larger mean $N_e$ is observed as compared to the mean $N_e$ expected from linear relation followed by region 1. It is due to the cut-off on $N_e$ by Level-1 trigger. When $E_T$ decreases, only those EAS can reach the detector which developed deeper in the atmosphere and are able to produce the trigger. This leads to higher values of mean $N_e$. To get energy-size relation, the profile plot is fitted with 2 different functions (4) and (5) in the region 1 and region 2, respectively.

$$logN_e = \frac{logE_T - A}{\alpha_1} \qquad ...(4) \qquad\qquad logN_e = (\tfrac{1}{\alpha_2}).ln\left(\frac{B - logE_T}{C}\right) \qquad ...(5)$$

where A, B and C are the fit parameters and $\alpha_1$ and $\alpha_2$ are fixed parameter. The values of $\alpha_1$ and $\alpha_2$ are set to 0.85 and -1.405, respectively. Zenith angle correction is done by parameterizing the values of A, B and C obtained from fitting. A, B and C vary linearly with sec$\theta$ as follows.

$$A = A_0 + A_1 sec\theta \qquad B = B_0 + B_1 sec\theta \qquad C = C_0 + C_1 sec\theta \qquad ...(6)$$

Fit values of $A_0$, $A_1$, $B_0$, $B_1$, $C_0$ and $C_1$ are -0.25, 1.52, 3.36, 1.98, 23.75 and 154.84, respectively. The reconstructed energy ($E_R$) can be calculated by the following relations:

$$logE_R = \alpha_1 . logN_e + A \qquad ...(7) \qquad\qquad logE_R = B - C.exp(\alpha_2 . logN_e) \qquad ...(8)$$

The energy resolution is calculated via the distribution of $logE_R$ - $logE_T$, called as Bias. Distribution of bias for $1.0 \leq \sec\theta < 1.05$ and energy bin $10^{3.8} - 10^4$ GeV and energy bin $10^{5.2} - 10^{5.4}$ GeV are shown in Figure 3(b) and Figure 3(c), respectively. The distribution is symmetric in region 1 while asymmetric in region 2. This asymmetry is due to the cut-off on $N_e$ by Level-1 trigger and results in favouring reconstruction towards the lower side. Energy resolution is calculated by $FWHM/2.354$ of the distribution of bias. Median value of energy bias and energy resolution as a function of $E_T$ are shown in Figure 3(d) and Figure 3(e), respectively. Error bars in Figure 3(d) represent the energy resolution. Energy bias is within 8% and energy resolution is 45% at 5 TeV and 8% at 10 PeV.

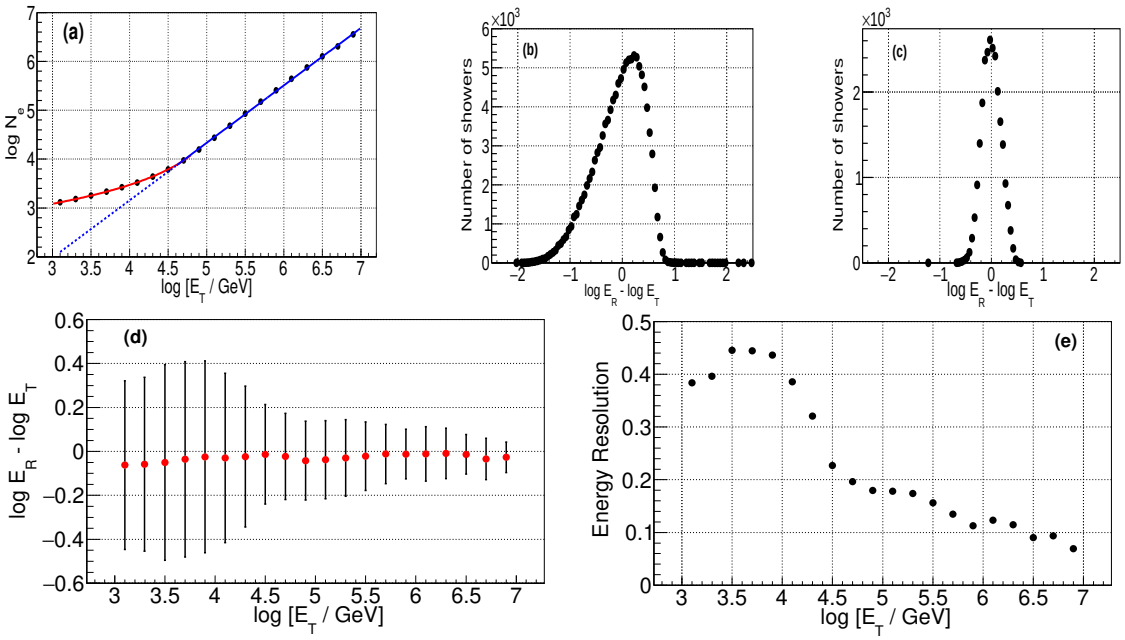


Figure 3: (a): Profile plot for true energy ($E_T$) and reconstructed size ($N_e$). Data points (•), fitting in region 1 with (4) (——), extrapolation of (4) in region 2 (- - -) and fitting in region 2 with (5) (——) are shown. (b) and (c): distribution of bias for energy bin $10^{3.8} - 10^4$ GeV and energy bin $10^{5.2} - 10^{5.4}$ GeV, respectively, (d): Variation of median value of energy bias as a function of $E_T$ and error bar represents energy resolution, (e): Variation of energy resolution as a function of $E_T$, all plots are for proton generated shower and $1.0 \leq \sec\theta < 1.05$.

## 4. Preliminary cosmic rays spectrum

The PCRs energy for data is reconstructed on event by event basis considering all particles to be proton, using the energy-size relation obtained from the simulation. Distribution of reconstructed energy ($E_R$) is obtained by taking the logarithmic bins of bin-width $10^{0.1}$. Since the EAS

development is influenced by the atmospheric paremeters, shower axis direction and type of PCRs, there is a large fluctuation in the measured $N_e$ (including detector response) for a given true energy of PCRs that leads to the smearing of $E_R$ (especially at lower energy). Therefore an iterative bayesian unfolding method presented in reference [5] is used to obtain the unfolded energy ($E_U$) distrubution from the distribution of $E_R$. The $\mathbf{p(E_R|E_T)^{MC}}$ is the smearing matrix which defines the probability of an EAS of energy $E_T$ to reconstruct with energy $E_R$. These probabilities are calculated by Monte Carlo (MC) simulation. If $\mathbf{N_T^{MC}}$ is a vector containing number of EAS in the distribution of $E_T$, and $\mathbf{N_R^{MC}}$ is the vector containing number of EAS in the distribution of $E_R$ in MC simulation, then $\mathbf{N_R^{MC}}$ is related to $\mathbf{N_T^{MC}}$ as

$$\mathbf{N_R^{MC}} = \mathbf{p(E_R|E_T)^{MC}}.\mathbf{N_T^{MC}} \qquad ...(9)$$

Figure 4(a) shows the smearing matrix calculated from the simulation. The palette represents the value of probability in a given cell. The smearing matrix is used to calculate the unfolding matrix $\mathbf{p(E_T|E_R)}$ by using bayes law as follow

$$\mathbf{p(E_T|E_R)} = \frac{\mathbf{p(E_R|E_T).p_o(E_T)}}{\Sigma_{E_T'}\,\mathbf{p(E_R|E_T').p_o(E_T')}} \qquad ...(10)$$

where $\mathbf{p_o(E_T)}$ is the intial prior vector for distribution of $E_T$. Since a suitable initial prior leads to fast convergence of the unfolding process, a power law distribution with spectral index of -1.7 is used to calculate the initial prior without any regularization. Equal probability and other priors of power law form are also tested. They also give the same results with negligible difference but take more iterations to converge. The vector ($\mathbf{N_T}$) for distribution of $E_U$ is calculated as

$$\mathbf{N_T} = \frac{1}{\varepsilon(\mathbf{E_T})}\Sigma_{E_R'}\mathbf{p(E_T|E_R')}.\mathbf{N_R'} \qquad ...(11)$$
$$\varepsilon(\mathbf{E_T}) = \Sigma_{E_R'}\mathbf{p(E_T|E_R')} \qquad ...(12)$$

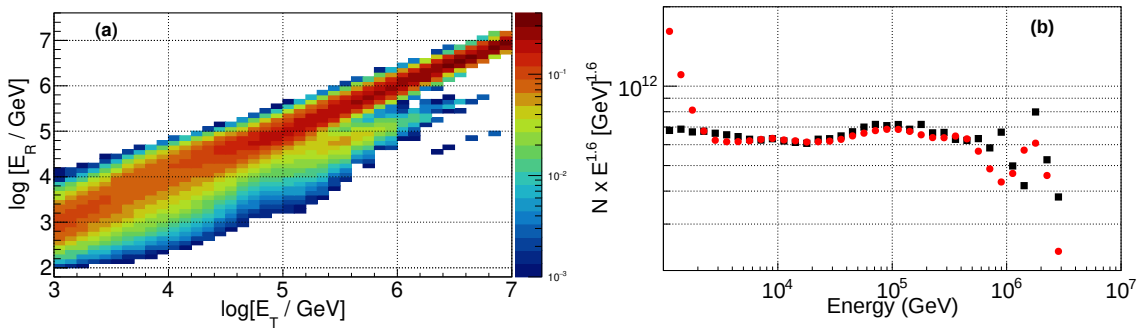


Figure 4: (a): Smearing matrix calculated from simulation, for unfolding process. (b): Comparsion of true distribution of simulated data(■) and unfolded distribution (●)

where $\mathbf{N_R}$ is the vector for distribution of $E_R$ and $\varepsilon(\mathbf{E_T})$ is the efficiency of observing a shower of energy $E_T$ for any of the $E_R$. The unfolding iteration starts with selection of a suitable prior, followed by calculation of $\mathbf{p(E_T|E_R')}$ and then calculation of $\mathbf{N_T}$. The posterior $\mathbf{p(E_T)}$ is calculated from $\mathbf{N_T}$. The prior is updated with posterior and next iteration starts. For analysis, the convergence condition for unfolding is $|max(\mathbf{p(E_T)} - \mathbf{p_o(E_T)})| \leq 0.001$. Before applying to data, the

performance and capability of the unfolding is tested with an independent simulated data set of proton initiated EAS of energy range 1 TeV to 3 PeV. The result of unfolding is shown in figure 4(Lower). The input distribution and unfolded distribution is represented by black and red filled circles respectively. In energy range ∼5 TeV to ∼150 TeV, there is good agreement between unfolding distribution and true distribution. The deviation at higher energy is due to the limiting statistics in simulation to calculate the smearing matrix. For data, the unfolding is used from 5 TeV to 150 TeV, but for $E_R > 150$ TeV, the limiting statistics in simulation and good energy resolution motivate us to obtain the spectrum directly from the observed reconstructed energy distribution. The differential cosmic-ray spectrum (dI/dE) is obtained as follows:

$$\frac{dI}{dE} = \frac{1}{T_{obs}} \left(\frac{N}{\Delta E.A}\right)_i \qquad ...(13)$$

where subscript i denotes the $i^{th}$ energy bin, N is the number of EAS, $\Delta E$ is the width of energy bin and $A_{acc}$ is acceptance for the $i^{th}$ energy bin. $T_{obs}$ is the live time of the data.

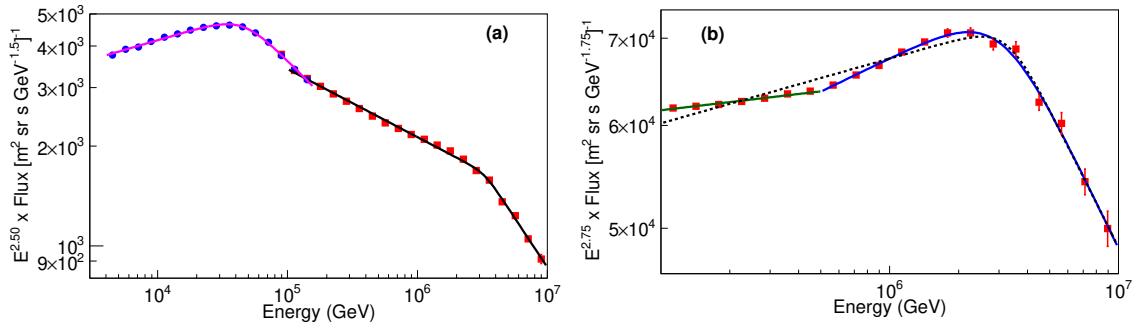


Figure 5: (a): Unfolded energy spectrum and spectrum generated by distribution of $E_R$ scaled with $E^{2.5}$ with broken power law fit. (b): Spectrum generated by distribution of $E_R$ scaled with $E^{2.75}$ with power law (green) and broken power law fit (blue), entire range is fitted with another power law (dashed black).

Figure 5(a) shows the unfolded (low energy) spectrum and the spectrum generated from distribution of $E_R$ (high energy), represented as blue filled circles and red filled squares, respectively. The statistical uncertainties are smaller than the marker size. The spectrum is scaled by $E^{2.5}$ and fitted with two broken power laws. One of the broken power laws (magenta) is used to fit low energy spectrum which results in $\gamma_1^{low}$ = -2.386 ± 0.002 and $\gamma_2^{low}$ = -2.898 ± 0.004 with an energy break $E_{br}^{low}$ at 45.4 ± 0.3 TeV. Other broken power law (black) is used to fit the high energy spectrum by assigning equal weight to each point which results in $\Gamma_1^{'}$ = -2.705 ± 0.004 and $\Gamma_2^{'}$ = -3.092 ± 0.066 with the knee $E_{br}^{'}$ at 3.3 ± 0.4 PeV. The values of the Knee, $\Gamma_1^{'}$ and $\Gamma_2^{'}$ is consistent with the KASCADE results, within error limits. Figure 5(b) shows the high energy spectrum and to highlight the fine structure near the knee, the spectrum is scaled by $E^{2.75}$. The spectrum is fitted with a power law in energy range 100 TeV to 600 TeV and a broken power law in the energy range 600 TeV to 10 PeV. The power law fit gives $\Gamma^{high}$ = -2.729 ± 0.001 while the broken power law results in $\gamma_1^{high}$ = -2.664 ± 0.007 and $\gamma_2^{high}$ = -3.116 ± 0.064 with the knee $E_{br}^{high}$ at 3.1 ± 0.3 PeV.

Figure 6 shows the combined spectrum obtained by GRAPES-3 along with spectrum obtained by other experiments. Blue and red filled circles represent the low and high energy spectrum,

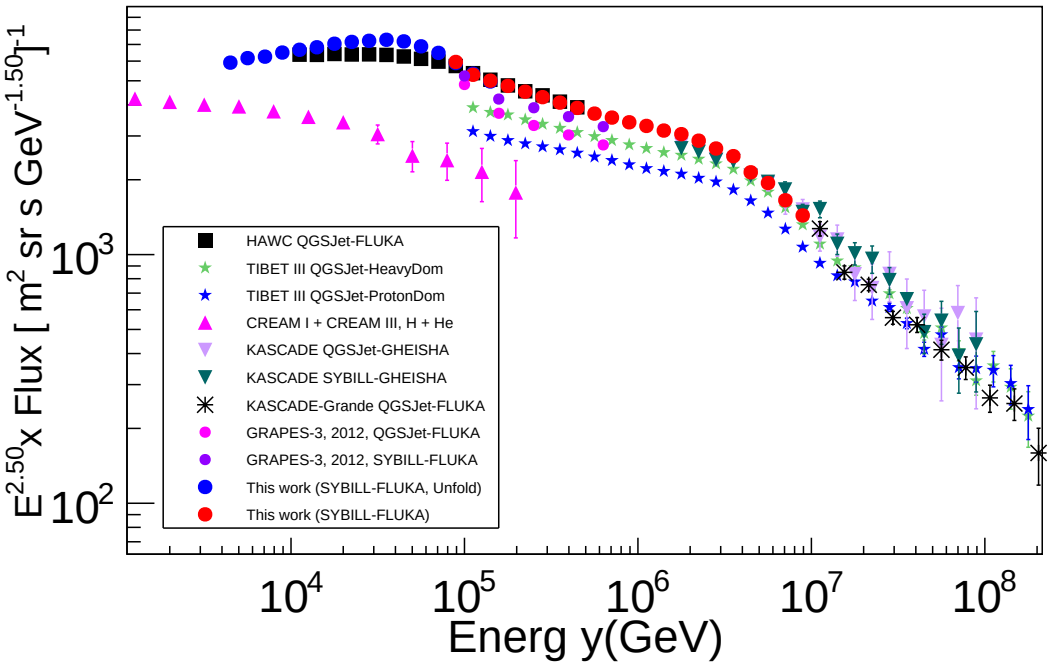


Figure 6: All particle energy spectrum scaled by $E^{2.5}$

respectively. Since the analysis is done by considering all particles to be proton, the absolute flux of GRAPES-3 unfolded spectrum is scaled by 2.37 and high energy spectrum by 1.6 in order to match with KASCADE all particle spectrum.

## 5. Acknowledgement

We thank D.B. Arjunan, S. Kingston, K. Manjunath, S. Murugapandian, B. Rajesh, M.S. Shareef, C. Shobana, R. Sureshkumar and other colleagues for their help in running and maintanence of the GRAPES-3 experiment.

## References

[1] S. K. Gupta et al., *Nucl. Instrum. Meth.* A 540 (2005) 311.

[2] P. K. Mohanty et al., *Astropart. Phys.* 31 (2009) 24.

[3] Y. Hayashi et al., *Nucl. Instrum. Meth.* A 545 (2005) 643.

[4] T. Ullrich and Z. Xu, arXiv.org/abs/physics/0701199v1

[5] G. D'Agostini, *Nucl. Instr. Meth.* A 362 (1995) 487.